Nanotechnology Center for Biomedical, Environmental and Sustainability Applications
A Center for Research Excellence in Science & Technology (CREST) at the University of Puerto Rico - Mayaguez
crest.uprm.edu
crest2.uprm.edu

The Mayagüez Nanotechnology Center: 10 Years of Transformative Impact on Interdisciplinary Research-The Highlights

O. Marcelo Suárez, Agnes M. Padovani-Blanco, Madeline Torres-Lugo, Arturo Hernández-Maldonado, and Oscar Perales-Pérez
University of Puerto Rico – Mayagüez

Abstract

Established in 2008 at the University of Puerto Rico – Mayagüez (UPRM), the Nanotechnology Center focuses on in-depth training of students from public schools, undergraduate and graduate students through research-intensive interdisciplinary activities. The Center's research structure encompasses 4 Interdisciplinary Research Groups (IRGs) focused on specific subjects but linked by the exploitation of new phenomena at the Nanoscale in areas related to nanomedicine, water cleaning and disinfection, and materials for sustainable applications. The outcomes of Phase I and II of the Center led to more than 500 posters and oral presentations, as well as near 150 peer-reviewed publications and graduation of dozens of graduate students. Through these ten years, the Center members obtained more than $25 million from federal agencies to expand the research and education impact.

IRG-1A (Leader: M. Torres-Lugo)

Optimization of the Thermal Chemopotentiation of Anticancer Drugs by Magnetic Fluid Hyperthermia for Cancer Treatment

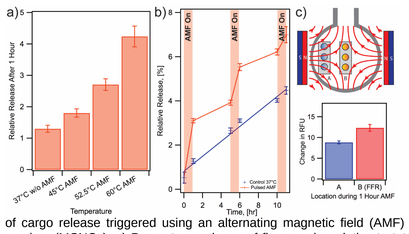

Demonstration of cargo release triggered using an alternating magnetic field (AMF) from magnetic composite nanocarriers (MCNCs). a) Percentage release of fluorescein, relative to total release after 10 h at 90°C, for passive conditions at 37°C and alternating magnetic field (AMF) triggered release under various target temperatures. b) MCNCs release cargo multiple times in response to successive applications of AMF. c) Use of selection magnetic field gradients controls MCNC cargo release. Samples located in the field free region (B in the drawing) release more cargo than samples located in the saturating field (A in the drawing).

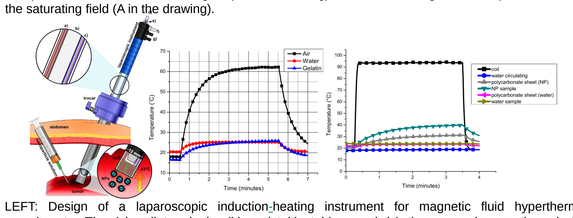

LEFT: Design of a laparoscopic induction-heating instrument for magnetic fluid hyperthermia experiments. The (a) coil terminals, (b) peristaltic tubing, and (c) thermocouples go through the instrument (tube). Also, five input/output accesses are included for the (d) peristaltic tubing, (e) thermocouples, (f) water, and (g) coil terminals. Once the peristaltic pump is turned on, water starts filling the interior of the instrument through (d), until it reaches the top, and exits through (f). The laparoscopic instrument would go through a trocar (like in laparoscopy) and would be directed to the tumor of interest. CENTER: Temperature profile of a stainless-steel disk exposed to a magnetic field intensity of 3 kA/m at 290 kHz in air, water, and gelatin media. RIGHT: Nanoparticles and water sample exposed to a magnetic field intensity of 15 kA/m at 290 kHz.

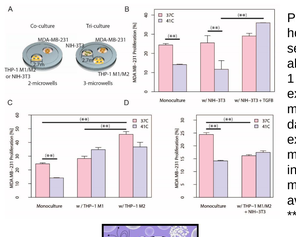

Proliferation levels in MDA-MB-231 after exposure to heat damage. A) Schematic representation of cell seeding layout. MDA-MB-231 cells were cultured alone (monoculture) and with (w/) NIH-3T3 (B), THP-1 (C) or both (D). Cells were cultured at 37°C or exposed to 41°C for 30 min. Proliferation was monitored at 48 hrs post-heat damage. Co-culture data represents average of two independent experiments with n=8 microwells. Tri-culture and monoculture data represents average of 3 independent experiments with n=8 and n=4 microwells, respectively. Data represents mean data average +/- 1 SE. Student t-test, *P<0.05, **P<0.005, ***P<0.001 and **** P<0.0001.

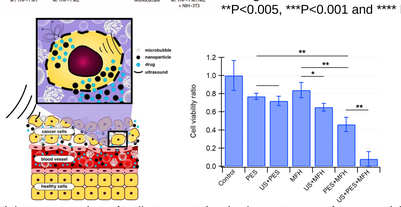

LEFT: Pictorial representation of cell sonoporation in the presence of nanoparticles and drug. RIGHT: Combination treatments using magnetic nanoparticles, pifithrin-μ and ultrasound to investigate effects on cellular uptake and viability. Sonicated cells were then exposed to external, alternating magnetic fields with intensities of 11 - 15 kA/m to achieve sustained temperatures of 41 or 43° C for 30 minutes. Our results show that combined US/MFH/pifithrin-μ treatments led to increased cancer cell death. In addition, the cell killing profile was higher than that of individual treatments when cells were treated with drug or MFH, respectively, and also higher than that of combined MFH/drug without exposure to ultrasound.

(1) Provisional patent: Laparoscopic Magnetic Field Generator for Magnetic Fluid Hyperthermia Applications; Inventor: Eduardo J. Juan et al.; Ser.#.: 62/462,623
(2) Provisional patent: Multi-Microwell array for multi-cellular adjacent co-culture; Inventor: Maribella Domenech and Karla P. Ramos; Ser. #: 62/293,836

IRG-1B (Leader: O. Perales-Perez)

Cytotoxicity of Zinc Oxide Nanoparticles in Modeled Microgravity Conditions (J. Acevedo, M. Latorre)

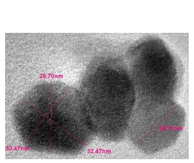

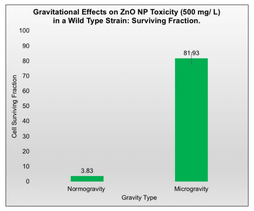

ZnO Nanoparticles produced by the sol-gel method show reduced toxicity towards the yeast *Saccharomyces cerevisiae* in modeled microgravity conditions.

In Vitro Cell Viability of Hormone Dependent MCF-7 Breast Cancer Cell Line in Presence of ZnO Nanoparticles Doped with Titanium (J. Carmona, O. Perales, E Melendez)

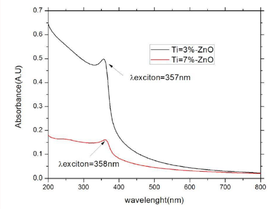

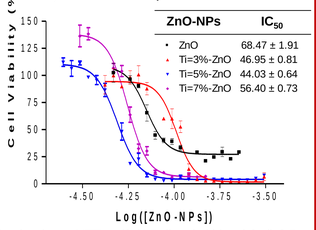

ZnO-NPs	IC_{50}
ZnO	68.47 ± 1.91
Ti=3%-ZnO	46.95 ± 0.81
Ti=5%-ZnO	44.03 ± 0.64
Ti=7%-ZnO	56.40 ± 0.73

Cytotoxicity of ZnO-NPs were determined by MTT (3-(4,5-dimethylthiazol-2-yl)-2,5-diphenyltetrazoliumbromide) colorimetric assay after 48 hours of NPs exposure. ZnO-NPs Photodynamic Properties could result in a selective non-invasive approach for breast cancer treatment

Surface Chemistry Dependence of Cytotoxicity of ZnSe(S) Quantum Dots Against Pancreatic Cancer and Normal Cells (E. Calderon, J. Rodriguez, O. Perales)

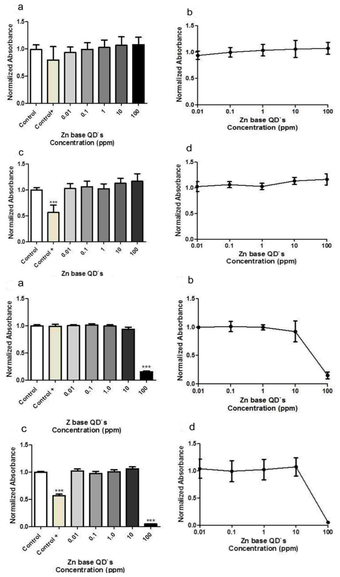

Water-stable ZnSe(S) Quantum Dots (QDs) were synthesized using Microwave heating in presence of thiol compounds, thioglycolic acid (TGA) and mercaptopropionic acid (MPA). The thiols would act as the source of sulfide species during the QDs synthesis as well as surface functionalization agents. The syntheses parameters included the reaction temperature and time (80°C-180°C, 10 minutes-60 minutes) and a suitable acidity of the aqueous medium. FTIR measurements evidenced the presence of thiol functional groups onto the QDs surface.

UPPER (a-d): The PANC-1 cell population was not affected when TGA-capped ZnSe(S), up to concentrations of 100 mg QDs/liter of cell suspension, was used both in pancreatic cancer (PANC-1). A similar trend was observed in healthy pancreas cells (RWPE-1).

DOWN (a-d): MPA-treated ZnSe(S) evidenced cytotoxicity against PANC-1 at a concentration as low as 10 mg QDs/liter of cell suspension. The lethal dose (LD50) for the MPA-capped ZnSe(S) was estimated for both, 24 and 48 hours at 36ppm and 35ppm in prostate cancer cell line (PC3) and 100ppm. The normal pancreas cells (RWPE-1) were less sensitive to this effect.

The strong effect of the surface chemistry of nanomaterials on their intrinsic cytotoxicity became evident.

IRG-2 (Leader: A. Hernandez)

Nanostructured Materials for Remediation of Recalcitrant and Emerging Contaminants Present in the Environment

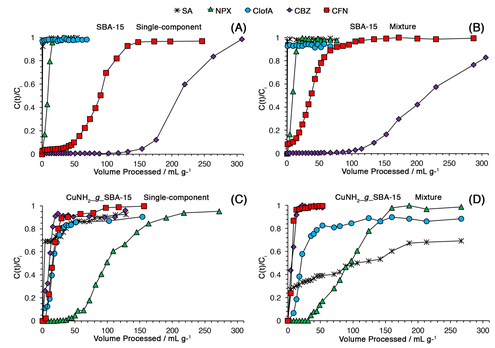

Breakthrough of selected contaminants of emerging concern (CECs) in fixed-beds with SBA-15 or $CuNH_2$_g_SBA-15, for water feed at 25 ℃ and neutral pH. CECs include salicylic acid (SA), naproxen (NPX), clofibric acid (ClofA), carbamazepine (CBZ) and caffeine (CFN). CECs fed as (A and C) single components and (B and D) fed as a mixture. Data gathered for Ci = 10 μg L^{-1}, Q = 1.5 mL min^{-1}, and H = 10.0 cm. Solid lines are for visual representation of the data. Abscissa units correspond to water volume processed per mass of adsorbent bed. **Source**: Hernandez-Maldonado and co-workers, 2018.

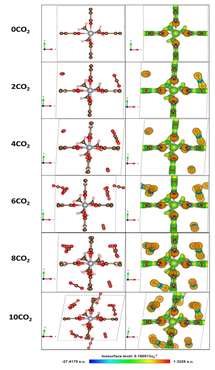

Deformed Ni(bdc)(ted)$_{0.5}$-nCO_2 (bdc: 1,4-benzene-dicarboxylate; ted: triethylenediamine) structures after full relaxation including their electrostatic potentials. The figure to the left shows the structures of the nanoporous metal organic framework (MOF Ni(bdc)(ted)$_{0.5}$ upon interaction with up to ten CO_2 molecules. It also shows the electrostatic potentials for each case. Our calculations suggest that the CO_2 molecules within the framework slightly modify the dimensions and electrostatic potential of the system. **Source:** Curet-Arana and co-workers 2018.

Environmentally friendly magnetic bio-nanocomposite for the removal of oxybenzone (BP-3) in water systems (V. Fernandez-Alos, O. Perales-Perez, and F. Roman-Velazquez)

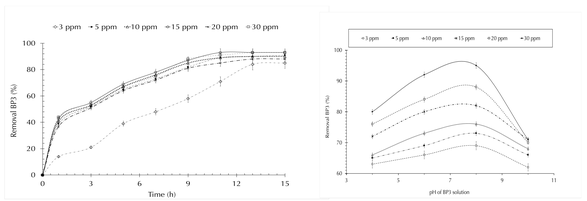

Effect of contact times for the adsorptive removal of BP-3 onto magnetic bio-nanocomposite at different initial concentrations; pH 8.04±0.02; absorbent load of 0.15g per 100 mL; equilibration time of 7h.

Effect of solution-pH on the removal of BP-3 by magnetic bio-nanocomposite at different concentrations; adsorbent concentration = 0.05 g/100 mL.

(1) Ortiz-Martínez, K.; Vargas-Valentín, D.A. ; Hernández-Maldonado, A.J. *Ind. Eng. Chem. Res.* **2018**, *57*(18), 6426-6439. DOI: 10.1021/acs.iecr.7b05168.
(2) Hernández-Maldonado, A.; Rivera-Jiménez, S.M.; Méndez-González, S. Novel Adsorption Material for Removing Chemical Compounds from Water and Method of Making the Same. US Patent 10,086,359 (2018).

IRG-3 (Leader: O. M. Suárez)

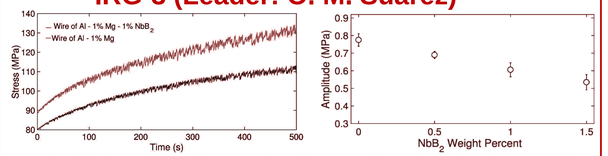

Attenuation of the dynamic aging phenomenon in solution-treated Al-Mg alloys using NbB_2 nanoparticles.

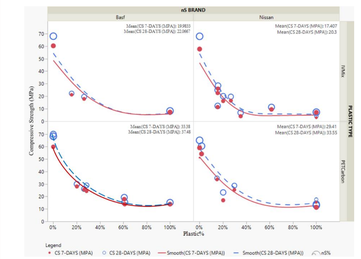

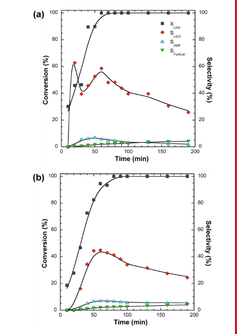

Compressive strength of nanomodified concrete proposed as structural material containing recycled plastic and different types of nanosilica.

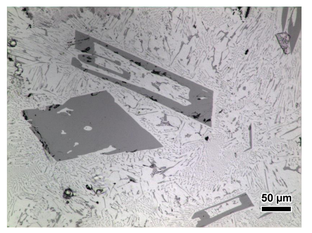

Optical image of the microstructure of the external surface of a centrifugally experimental Al - 14wt.% Ce sample. The 500 RPM rotational speed allowed segregating the largest intermetallic particles of this near-eutectic alloy intended for aerospace applications.

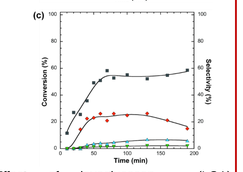

Effect of levoglucosan (LGA) concentration on the dehydration of LGA using endcapped SiliaBond®-PSA catalyst in THF at 483 K and 69 bar He and LGA concentrations of (a) 14 mM, (b) 36 mM and (c) 89 mM. The acid loading was kept at 0.08 mmol H^+.

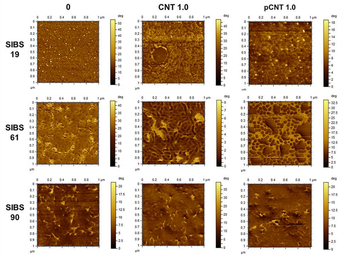

AFM phase images for the sulfonated and Poly (styrene - isobutylene - styrene) nano-composites membranes with maximum nanofiller loadings.

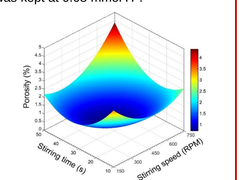

Response surface of porosity as a function of the stirring time and speed used in the optimization of aluminum filler reinforced with nanoparticles

Atrazine residual levels upon exposure to a glass / nano-structured titanium dioxide composite with different particle size

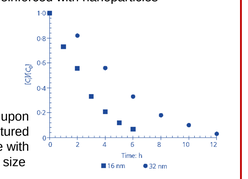

(1) Declet-Vega, A.; Sepulveda-Ramos, N.; Martinez-Santos, J.; Suarez, O. M. Study of Electrical Properties of Biocomposites Containing Ferroelectric Nanoparticles. *J. Compos. Mater.* **2016**, *51* (14), 1979–1985.
(2) Declet-Vega, A.; Sepúlveda-Ramos, N.; Suárez, O. M. On the Mechanical and Dielectric Properties of Biocomposites Containing Strontium Titanate Particles. In *Ferroelectrics and Their Applications*; Irzaman, H., Ed.; Intechopen Ltd.: London, UK, 2018; pp 73–88.
(3) Oyola-Rivera, O.; González-Rosario, A. M.; Cardona-Martínez, N. Catalytic Production of Sugars and Lignin from Agricultural Residues Using Dilute Sulfuric Acid in γ-Valerolactone. *Biomass and Bioenergy* **2018**, *119*, 284–292. doi: 10.1016/j.biombioe.2018.09.031.
(4) Ruiz-Colón, E.; Pérez-Pérez, M.; Suleiman, D. Influence of Carboxylated and Phosphonated Single-Walled Carbon Nanotubes on the Transport Properties of Sulfonated Poly(styrene-isobutylene-styrene) Membranes. *J. Polym. Sci. Part A: Polym. Chem.* **2018**, *56*, 2475-2495. doi:10.1002/pola.29222
(5) Avilés, A.; Hernandez, C.; Ambrose, J.; Suárez, O. M.; Tarafa, P. J. Degradation of Atrazine with Titanium Dioxide Immobilised in Compact Recycled Glass. *J. Environ. Eng. Sci.* **2017**, *12* (4), 79–85.

This material is based upon work supported by the National Science Foundation (NSF) under Grants HRD 0833112 & 1345156 (CREST program).